Integration of an Optical Hydrophone with a High Dexterity Robot for End Effector Localization

Stephen Van Kooten

May 14, 2013

Abstract

A system was partially developed to locate the end effector of the APL Snake robot [1] by way of an integrated optical hydrophone and externally applied ultrasound signal. In addition, algorithms were developed for calibration of the system, and a brief analysis of error tolerances was conducted. A Python wrapper for an electromagnetic tracker interface was also developed.

1 Background

The goal of this project was to develop a means to track the position of the end effector of the APL Snake robot, a high-dexterity robotic manipulator intended to be used in removal of osteolytic bone from cavities that form behind the cup of a hip implant. For the current design of the snake robot, an accuracy of only 1.3 mm can be obtained by estimating tip location through the robot kinematics. There is a desire to increase this accuracy by direct tracking, particularly because future models of the Snake robot may have more complicated kinematics, further decreasing the accuracy of kinematic estimation.

Though several methods of tracking robotic manipulators currently exist, the design of the robot and its intended use make these methods difficult or impossible. The manipulator itself consists of many coplanar joints, so to accurately track the end location the position of the last segment is required. However, the last segment will be wholly within an internal cavity, so there is no line of sight for optical tracking. The end manipulator itself is made of metal, so an electromagnetic tracking system would see a large degree of distortion. The cavity in which the robot works is surrounded by bone, which is sufficiently thick to prevent tracking through ultrasonic imaging.

Although normal ultrasonic imaging does not work because there is a large reflection coefficient and the signal must penetrate the bone twice to image, it may be possible to detect a one-way signal from a receiver in the cavity.

2 Solution

Our solution for tracking the end manipulator consists of using an optical hydrophone to sense an ultrasound signal originating from a linear array probe placed on the patient's lower back and aimed through the back of the acetabulum. An optical hydrophone was used because it is sufficiently small to be integrated into the end manipulator in the Snake robot through a small channel that runs the length of the manipulator. The optical hydrophone consists of a fibre optic cable terminated with a Fabry-Perot interferometer. A laser is sent through the fibre and the measured reflectance would be used to estimate the intensity of an ultrasound signal.

The hydrophone and ultrasound probe would be used to locate the end effector by measuring the time of flight of an ultrasound signal from the probe to the hydrophone and using an estimated speed of sound to calculate the distance between the two. With the distance from the hydrophone to several known locations, the location of the hydrophone may be calculated by multilateration.

Linear array ultrasound probes consist of an array of piezoelectric elements located in a colinear array. To unambiguously determine the location of the hydrophone, readings from two probe orientations are required.
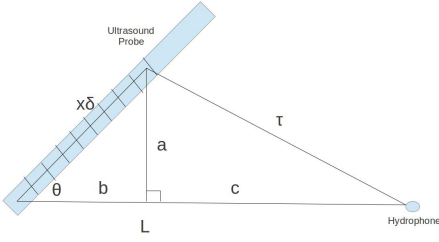
Figure 1: Single reading geometry.

3 Reading a frame of data

Due to the linear configuration of the ultrasound array, some error can be mitigated if the geometry is taken into account for each set of measurements in a single probe position and orientation.

See Fig. 1 above for probe and hydrophone geometry, where x is the zero-based index of the element emitting an ultrasound pulse, L is the distance from the hydrophone to the first element, δ is the spacing between elements, and τ is the distance from the current element to the hydrophone calculated from the time of flight of the ultrasound signal. We have the following relations:

$$\tau^2 = a^2 + c^2$$

$$L = b + c$$

$$a = x\delta \sin\theta$$

$$b = x\delta \cos\theta$$

$$
\begin{aligned}
\tau^2 &= a^2 + c^2 \\
&= (x\delta \sin\theta)^2 + (L - b)^2 \\
&= x^2\delta^2 \sin\theta^2 + L^2 - 2Lx\delta\cos\theta + x^2\delta^2\cos\theta^2 \\
&= L^2 - 2Lx\delta\cos\theta + x^2\delta^2
\end{aligned}
$$

Given the equation for τ^2 above and a set of measurements with their corresponding element index, we can estimate the unknown parameters with non-linear least squares. The Gauss-Newton method was used to estimate the parameters L, δ, and $\cos\theta$

4 Registration to EM tracker

Although the ultrasound probe can be tracked by the EM tracker, there is a need to determine the location of the ultrasound array in the probe in the frame of
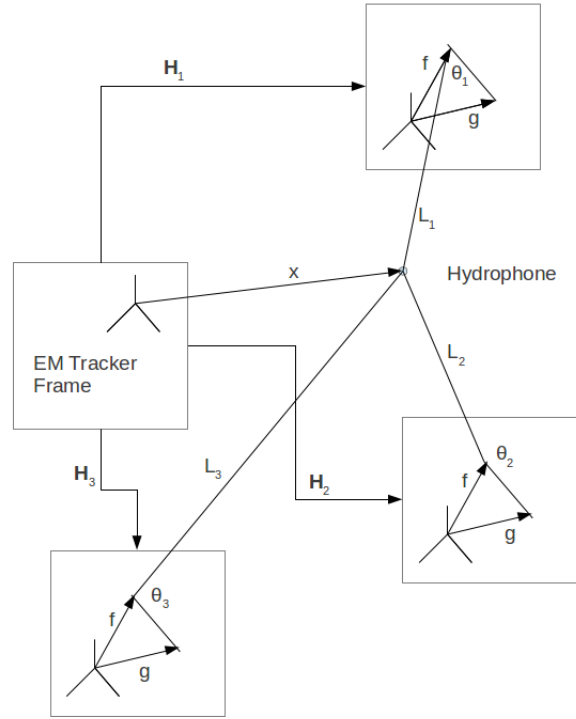

Figure 2: EM-to-ultrasound geometry.

the EM marker. Although techniques exist for doing this by imaging a calibration object, it would be useful to simplify calibration by using the hydrophone, eliminating the need for a specialized calibration object.

Calibration would be done by placing the hydrophone in a water bath, using an EM pointer and pivot calibration to find its position in EM tracker coordinates ($\vec{x}$), and then taking multiple ultrasound time-of-flight readings with the probe in different positions. For each set of ultrasound readings, a transformation, H_i, from the EM tracker frame to the frame of the EM marker would be obtained. For each set of readings in a single position, the single reading pre-processing step presented in Section 3 is used to obtain an L_i and $\cos\theta_i$.

The goal of calibration is to determine the position and orientation of the ultrasound array, so it was chosen to calculate two vectors: $\vec{f}$, a vector to the first element of the array, and $\vec{g}$, a vector to a point one unit along the length of the array from the first element (Fig. 2).

There are then six unknowns and each reading gives two values, so at least three readings are required for calibration. For the equations below, let $\vec{x} = 0$ which can be obtained by translating the EM frame before finding H_j.

There are two equations for each reading ($j \in [1..n]$):

$$\|H_j \vec{f}\| = L_j^2$$

$$(H_j \vec{g} - H_j \vec{j}) \cdot (H_j \vec{f}) = L_j \cos\theta_j$$

Fortunately we can further simplify these equations by using the fact that the dot product is invariant under rotations, that is for a rotation $\mathbf{R}$:

$$(\mathbf{R}\vec{u}) \cdot (\mathbf{R}\vec{v}) = \vec{u} \cdot \vec{v}$$

We then pre-extract the translational component ($\vec{t}$) out of the transformation H_j via:

$$H_j \vec{f} = \mathbf{R}\vec{f} + \vec{p} = \mathbf{R}(\vec{f} + \mathbf{R}^T \vec{p}) = \mathbf{R}(\vec{f} + \vec{t})$$

$$\vec{t}_j = \mathbf{R}_j^T \vec{p}_j$$

Applying the above simplification to the above we obtain:

$$\begin{aligned}
\|H_j \vec{f}\| &= L_j^2 \\
(H_j \vec{f}) \cdot (H_j \vec{f}) &= L_j^2 \\
(R_j(\vec{f} + \vec{t}_j)) \cdot (R_j(\vec{f} + \vec{t}_j)) &= L_j^2 \\
(\vec{f} + \vec{t}_j) \cdot (\vec{f} + \vec{t}_j) &= L_j^2 \\
\sum_i^3 f_i^2 + 2 f_i t_{(j)i} + t_{(j)i}^2 &= L_j^2
\end{aligned}$$

$$\begin{aligned}
(H_j \vec{g} - H_j \vec{j}) \cdot (H_j \vec{f}) &= L_j \cos\theta_j \\
(R_j(\vec{g} + \vec{t}_j) - R_j(\vec{j} + \vec{t}_j)) \cdot (R_j(\vec{f} + \vec{t}_j)) &= L_j \cos\theta_j \\
(R_j(\vec{g} - \vec{f})) \cdot (R_j(\vec{f} + \vec{t}_j)) &= L_j \cos\theta_j \\
(\vec{g} - \vec{f}) \cdot (\vec{f} + \vec{t}_j) &= L_j \cos\theta_j \\
\sum_i^3 g_i f_i - f_i^2 + (g_i - f_i) t_{(j)i} &= L_j \cos\theta_j
\end{aligned}$$

where j denotes the measurement frame and i denotes the ith element of a vector. Now the non-linear terms can be eliminated by subtracting the equation for each frame by the proceeding frame (frame 1-2, 2-3, 3-1), yielding:

$$\sum_i^3 2 f_i(t_{(j)i} - t_{(j+1)i}) + t_{(j)i}^2 - t_{(j)i}^2 = L_{(j)}^2 - L_{(j+1)}^2$$

$$2(\vec{t}_{(j)} - \vec{t}_{(j+1)})^T \vec{f} = L_{(j)}^2 - L_{(j+1)}^2 + \|\vec{t}_{(j+1)i}\| - \|\vec{t}_{(j)i}\|$$

Repeating this for the other set of equation yields:

$$(\vec{t}_{(j)} - \vec{t}_{(j+1)})^T (\vec{g} - \vec{f}) = L_{(j)} \cos\theta_{(j)} - L_{(j+1)} \cos\theta_{(j+1)}$$

For three readings the system is in the form of a system of six linear equations in six unknowns and can be solved by normal means. Note that additional calibration measurements could be accommodated with linear least squares if results are not sufficiently accurate.

5   Methods

Although the full system with time-of-flight measurement of ultrasound was not completed, we did test the algorithms in silico. To get reasonable results, the hardware as described below was tested to find the typical error rates of measurements.

5.1   Timing error

A circuit was constructed to time the electronic pulses on the TTL line of the ultrasound machine that occur whenever an element emits a pulse. The times were recorded by an Arduino Uno prototype board running at 16MHz, giving it a 62.5 ns time resolution. The ultrasound machine was set up to pulse every 70 μs and this period was compared to the Arduino's measured time between pulses. It was found that the maximum error during normal operation was within 4 clock pulses, corresponding to 250 ns error.

5.2   EM tracker pivot calibration

A Python wrapper was written to allow use of the EM tracker software within a Python environment. A pointer was constructed by attaching an EM marker to an ultrasound probe and affixing a pencil to the probe, the tip of which was used to pivot. A sheet of paper was printed with a 4×4 grid with a 30 mm square grid size and was affixed to a flat table. The EM tracker was then used to perform pivot calibration about each vertex of the grid. A rigid body transform was then calculated between the measured points and the known position of each grid point. This transform was then applied to the measured data to bring it into the frame of the known values and the values were compared. As shown in Figure. 3, the blue points are the known values, the red points are the measured values, and all axes are in millimetres.

5.3   Single frame reading

A simulation was done using the error rate found for the time measurement. One hundred probe positions/orientations were randomly generated such that
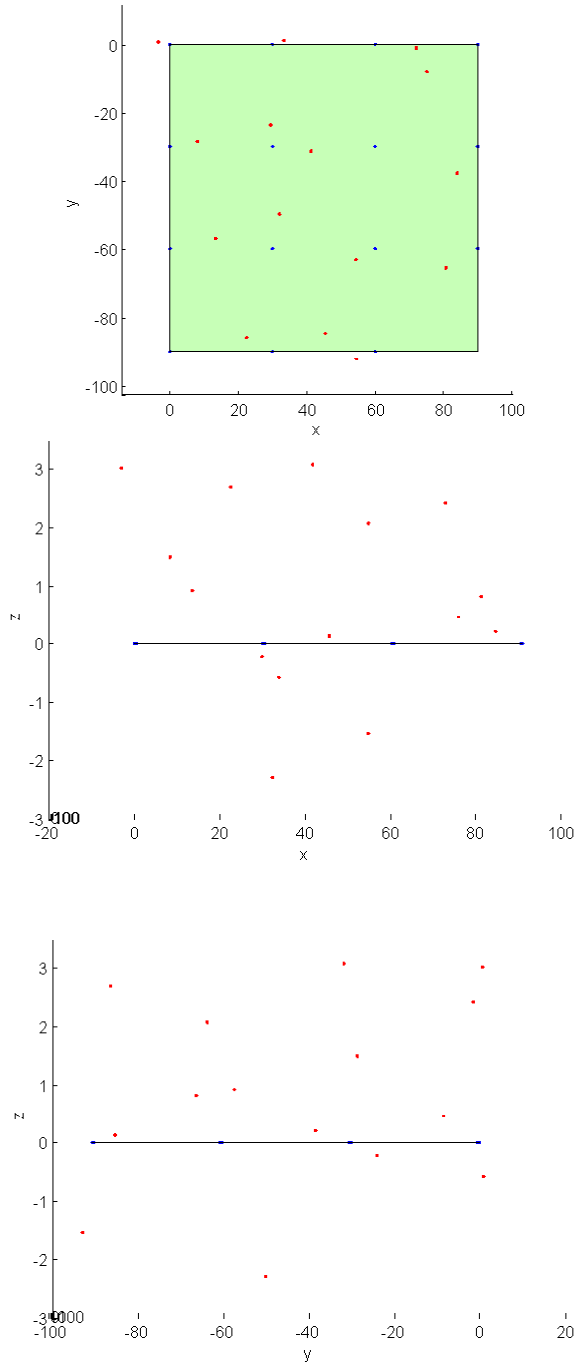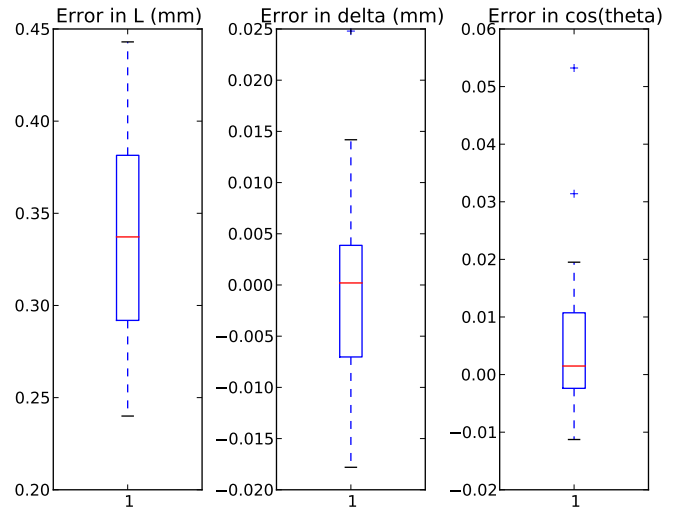
Figure 4: Single reading errors.

the distance of the first element to the hydrophone was uniformly distributed between 20 cm and 60 cm, distances typical of actual use case. For each sample an element spacing was randomly generated from a uniform distribution between 0.4 and 0.6 mm, similar to the 0.5 mm spacing of the ultrasound probe that we had intended to use. For each configuration, the unknown parameters were estimated and the error to the true values was calculated as shown in Fig. 4.

5.4 EM to US calibration

The algorithm presented in Section 4 was implemented in a simulation. The same errors as for the single frame reading simulation were used, but an additional error was added accounting for inaccurate pivot calibration of the hydrophone. For each run, ten randomly generated readings were used to calibrate the system. One thousand calibrations were performed with random hydrophone position errors and the relation between hydrophone position error and calibration error was found (see Fig. 5).

One thousand calibrations were then performed with zero offset due to hydrophone position error and the distribution of calibration error was found (see Fig. 6).

6 Use case scenario

The entire system is not yet complete, but a description of the use case scenario is presented below. It is

Figure 3: Error in electromagnetic tracking. Blue points are known, red points are measured by EM tracker.
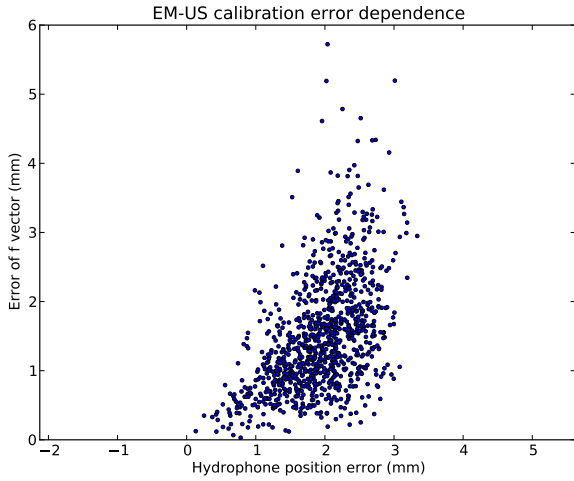
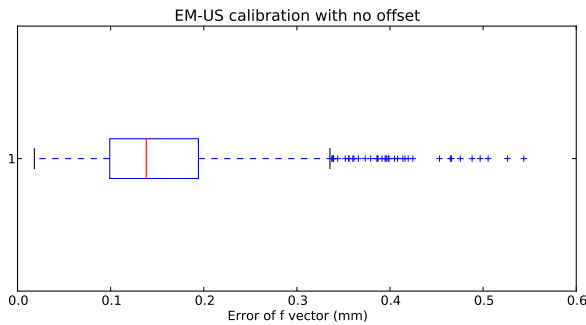Figure 5: Error dependence for EM to US calibration.

Figure 6: Calibration error without hydrophone position error.

assumed that there is an EM marker on the ultrasound probe and that the hydrophone is already integrated into the APL Snake robot end manipulator.

1. The end manipulator is inserted into a water bath.

2. An EM pointer is used to perform pivot calibration to determine the hydrophone location.

3. The ultrasound probe is placed in acoustic contact with the bath and pointed towards the hydrophone. Time-of-flight and EM readings are taken with the probe in at least 3 orientations.

4. The algorithm presented in Section 4 is performed to locate the ultrasound array in the ultrasound probe frame.

5. The robot end manipulator is inserted into the patient's osteolytic bone cavity and the procedure is performed normally.

6. During the procedure the surgeon or assistant would move the ultrasound probe back and forth along the patient's lower back directed towards the end manipulator. Readings are taken and the manipulator tip location is calculated through multi-lateration.

7. A monitor in the operating room would display a model of the cavity created from CT data and would display the tracked position of the manipulator tip in the scene. Visual markers could also show the volume the tip has reached, allowing the surgeon to see where additional bone removal is necessary.

7 Results

It was found that the single reading preprocessing was able to accurately determine the distance, orientation, and element space of the probe. The estimate for L wasn't significantly reduced compared to the 0.385 mm error from timing errors. However, the algorithm was able to determine the element spacing at a micron scale, potentially allowing the use of this technique to calibrate probes for which the exact element spacing is not accurately known.

From the results it appears that the EM tracker is extremely inaccurate. However, the tracker is rated for 2 mm accuracy, so the errors seen are most likely due to distortion. The test was conducted on a crowded

lab desk with multiple computers, an ultrasound machine, and a motor nearby, so it is not unreasonable to expect a large degree of distortion. This is further evidenced by the pattern of the errors seen in Fig. 3. For large negative y values and small x values there is a clear tendency for error in the positive x direction. The nearest metal object was in that part of the workspace, so it may account for the distortion. It should also be noted that there are relatively smaller errors in the z direction and there were no pieces of metal above or below the workspace.

For the calibration of the EM tracker to the ultrasound probe it was found that there is a rough linear relationship between hydrophone position error and calibration error with a slope close to unity. This suggests that the calibration accuracy is strictly limited by the accuracy of the system that tracks the ultrasound probe and determines the hydrophone position. However, for a perfect tracking system and the timing errors inherent to our system, we were able to achieve satisfactory calibration error (Fig.6) with a mean offset of 0.14 mm.

8 Conclusion

We have developed algorithms for using an ultrasound probe to track a hydrophone and shown ways to calibrate the system. Results from simulation have shown that these methods are robust against errors typical of the presented application, and it remains to be seen whether this technique could be applied to other noisier systems. In a system in a medical setting, higher accuracy EM or optical systems could be expected and higher frequency microprocessors would reduce errors introduced from limited temporal resolution, so we could expect even greater accuracy than presented here. One problem not addressed is that the speed of sound along the path of the ultrasound is not known exactly *a priori*. However, CT models could help predict the amount of bone the ultrasound will traverse and give an estimate on the average propagation rate. Furthermore, additional parameters could be introduced to the preprocessing step of each reading to estimate the speed of sound for different regions of the probe. The techniques presented could potentially be used with any linearly arranged signal source and point receiver. Notably there is no requirement that a typical medical imaging ultrasound probe be used. In fact a less specialized ultrasound source without geometri-

cally focused elements would be more ideal as it would allow the hydrophone to read the signal in a larger region and eliminate the need to accurately point the probe at the hydrophone.

9 State of the project and what I learned

I was the only student in my group so I did all of the work. I worked with Xiaoyu Guo to a limited extent, but I probably should have relied on his experience with the hydrophone more than I did, as I was not able to get the hydrophone to reliably pick up the ultrasound signal.

I did not reach my minimum deliverable of being able to locate the APL snake robot within 5 mm, as I fell behind schedule and was unable to get the hydrophone to reliably pick up the signal from the ultrasound probe. However, the algorithms for calibration are all implemented in the Python programming language, including a wrapper for the MEDsafe EM tracker.

I spent a significant amount of time working on reliably detecting the voltage pulse from the ultrasound machine that signals that an ultrasound pulse was emitted. I had initially intended to use an operational amplifier based voltage follower, but found that the slew rate on most commercial op amps was so low that very little signal was obtained. I then implemented an RS latch to detect the pulse and hold a voltage high until read. However, I had issues matching the impedance of the circuit with the ultrasound machine signal. Ultimately I found that just using the raw input and the interrupts on the Atmega chip the Arduino uses was sufficient to pick up the signal. In solving this problem I learned a good deal about the speed limitations of electronics that I normally think of as extremely fast.

For the project I had wanted to do the programming in Python as it is an interpreted language so I didn't have to deal with compilation and because the Python Numpy library is convenient for linear algebra. To that end I had to write a Python wrapper for the MEDsafe EM tracker software so I could control the EM tracker and acquire readings from within Python. I had never written a software wrapper before, so I learned some useful techniques from the experience.

10 Appendix

The Python wrapper code for the EM tracker software is uploaded to the project website (`https://ciis.lcsr.jhu.edu/dokuwiki/doku.php?id=courses:446:2013:446-2013-12:446-2013-12`).

References

[1] Michael DM Kutzer, Sean M Segreti, Christopher Y Brown, Mehran Armand, Russell H Taylor, and Simon C Mears. Design of a new cable-driven manipulator with a large open lumen: Preliminary applications in the minimally-invasive removal of osteolysis. In *Robotics and Automation (ICRA), 2011 IEEE International Conference on*, pages 2913–2920. IEEE, 2011.